Water-assisted extrusion and injection moulding of composites with surface-grafted cellulose nanocrystals – An upscaling study

(article starts on next page)

Water-assisted extrusion and injection moulding of composites with surface-grafted cellulose nanocrystals – An upscaling study

Lilian Forsgren [a,*], Abhijit Venkatesh [a], Florian Rigoulet [b], Karin Sahlin-Sjövold [b,c], Gunnar Westman [b,c], Mikael Rigdahl [a], Antal Boldizar [a]

[a] *Department of Industrial and Materials Science, Chalmers University of Technology, SE-412 96, Gothenburg, Sweden*
[b] *Department of Chemistry and Chemical Engineering, Chalmers University of Technology, SE-412 96, Gothenburg, Sweden*
[c] *Wallenberg Wood Science Center, Chalmers University of Technology, SE-412 96, Gothenburg, Sweden*

ARTICLE INFO

ABSTRACT

The large-scale surface modification of cellulose nanocrystals (CNC) was carried out to produce CNC-containing composites, in a scale of 3 kg, using industrial-scale melt processing techniques such as twin-screw extrusion and injection moulding. Two different polymer matrices, ethylene-acrylic acid copolymer (EAA) and low-density polyethylene (LDPE), were reinforced with 10 wt% unmodified cellulose nanocrystals (CNC) or surface-treated CNC, where a 2-hydroxyproyl-N-diallyl group had been grafted onto the sulphate half-ester groups on the CNC surfaces. This was achieved by mixing an aqueous CNC dispersion and the polymer pellets directly in the twin-screw extruder followed by a second dry compounding step prior to shaping by injection moulding. The injection-moulded materials were characterized with respect to their mechanical properties and thermal stability. The addition of 10 wt % CNC resulted in all cases in an increase in the yield strength and stiffness by 50–100%, most significantly for the EAA based composites. There were indications of the presence of a stable interphase and a percolating network in the EAA-based materials, according to dynamic-mechanical measurements. A reduction in thermal stability was observed for the melt-processed samples containing diallyl-modified CNC and discoloration in the EAA based samples.

1. Introduction

There is a drive towards a more sustainable society with a reduction in the use of fossil-based materials. At the same time, there is a need to use light-weight engineering materials to reduce energy demands in e.g. the transport section. A possible way to address both these concerns could be to use lignocellulosic materials as fillers/reinforcements. This has been recognized for many years, but there is a renewed interest due to the commercial availability of nanocellulose [1]. Cellulose nanocrystals (CNC) are especially interesting due to their highly crystalline nature, high stiffness, modest aspect ratio (less tendency to form agglomerates than cellulose nanofibers), large surface area, low toxicity, renewability, biodegradability and low abrasion to processing equipment [2–8].

Several studies indicate improvements in the mechanical performance by the addition of CNC to composites, but the results are difficult to compare due to the differences in properties of CNC from different fibre sources and by different production method used. The main method of producing nanocellulose composites has been through solvent casting, which is only viable on a laboratory scale [9–11]. In order to make the production of CNC-based composites commercially interesting on an industrial scale, the feasibility of using a conventional melt processing technique should be considered [12–14]. The mechanical properties of CNC composites are strongly dependent on the processing method used. Traditionally, the production of polymer composites on a large scale consists of two steps: mixing of the reinforcing element with the matrix followed by melt shaping processing method such as extrusion or injection moulding. In the case of cellulose nanocomposites, this may be either a batch- or a continuous-process. The latter is preferred due to its compatibility with existing industrial melt-processing methods. A master-batch approach is often used, where a dry mixture of nanocellulose is compounded with a polymeric carrier, and this master batch is then diluted with the matrix polymer and subsequently shaped via single-screw extrusion or injection moulding. The shear forces generated during the mixing and compounding operations should lead to a dispersive and distributive mixing of the components but there

is a risk that undesirable filler aggregation may occur [15,16]. However, it has been shown that water-assisted extrusion can reduce the degree of aggregation and this may facilitate the compounding step [17]. Herrera et al. have shown that water-assisted extrusion using cellulose nanofibers and chitin nanocrystals in a polylactic acid matrix improved the dispersion and mechanical properties [17,18]. Another advantage may be that the discoloration can be reduced by the presence of water in the system [19–21]. Chemical modification and compatibilization are also possible ways to reduce the problems [4,12,22–24]. Börjesson et al. showed that the onset temperature of thermal degradation of CNC was raised by almost 100 °C by grafting azetidinium salts onto the sulphate ester groups on the surface of the CNC [25]. When such surface-modified CNC was added to an ethylene acrylic-acid copolymer matrix both mechanical properties and thermal stability were improved [11].

In the present work, surface-modification and water-assisted melt processing has been combined to obtain CNC-reinforced composites. The production of cellulose nanocomposites has been upscaled from a laboratory scale using conventional large-scale melt processing techniques such as twin-screw extrusion and injection moulding. The large-scale production of N-diallyl-2-hydroxypropyl modified CNC was achieved by conjugation of N-diallyl carbonate reagent to the sulphate half esters on the CNC surface. Both modified and unmodified composites with CNC were produced by large-scale water-assisted mixing with a twin-screw extruder (TSE) followed by an additional compounding with a second pass through the TSE, followed by shaping into plaques via injection moulding (IM). Four different composites were produced, using unmodified CNC or CNC surface-modified with diallyl functionalities in either a poly (ethylene-acrylic acid) copolymer (EAA) or a low density polyethylene (LDPE) matrix. The mechanical, thermal and rheological properties of the composites obtained were compared with those of the EAA and LDPE matrices.

2. Material and methods

2.1. Materials

Sulphuric-acid-hydrolyzed cellulose nanocrystals (CNC) were obtained as a powder dispersible in water from Celluforce, Canada. The CNC powder was dispersed in water to a 6–7% dry content, using an IKA T25 digital Ultra Turrax at a rotational speed of 7400 rpm for 10 min. The diallyl surface modification of the CNC was based on a procedure outlined by Sahlin et al. but to access larger quantities with acceptable quality of N-diallyl-2-hydroxypropyl substituents, a new process was developed [26]. Instead of an azetidinium salt, a cyclic carbonate reagent (4-((diallylamino)methyl)-1,3-dioxolan-2-one) was used, synthesised via a two-step sequence, inspired by the procedures outlined by Reddy and Parzuchowski [27,28]. Epichlorohydrin (41.63 g, 450 mmol) was added dropwise for 3 h to a 1 L round-bottomed flask placed in an ice-bath, containing 250 mL of isopropanol and diallylamine (38.86 g, 400 mmol). The mixture was stirred at room temperature for 21 h, after which the solvent was removed under reduced pressure, and the crude product was confirmed to be 1-chloro-3-(diallylamino)propan-2-ol by NMR.

2.1.1. *NMR analysis of 1-chloro-3-(diallylamino)propan-2-ol*
^{1}H NMR (400 MHz, CDCl$_3$). δ = 5.82 m (=**CH**), 5.18 broad t (=**CH$_2$**) (*J* = 16 Hz), 3.89 broad dddd (**CH**OH) (*J* = 7 Hz), 3.52 m (**CH$_2$**Cl), 3.25 m (**CH$_2$**), 3.08 dd (**CH$_2$**) (*J* = 8, 16 Hz), 2.55 m (**CH$_2$**).
^{13}C NMR (101 MHz, CDCl$_3$). δ = 134.32 (=**CH**), 119.46 (=**CH$_2$**), 67.19 (**C**HOH), 57.06 (**CH$_2$**), 56.12 (**CH$_2$**), 47.10 (**CH$_2$**Cl) ppm.

The crude product was diluted in 1.2 L of acetonitrile, sodium bicarbonate (100 g, 0.6 mol) was added and the reaction was heated to reflux at approximately 85 °C for 16 h. The reaction mixture was filtered and rinsed with acetonitrile and the filtrate was concentrated under reduced pressure to yield a product which was confirmed to be 4-((diallylamino)methyl)-1,3-dioxolan-2-one by NMR.

2.1.2. *NMR analysis of 4-((diallylamino)methyl)-1,3-dioxan-2-one*
^{1}H NMR (400 MHz, DMSO-d_6). δ = 5.77 dddd (=**CH**) (*J = 6, 6, 10 and 17 Hz*), 5.17 dddd (=**CH$_2$**) (*J = 1, 1, 7 and 12 Hz*), 4.75 dddd (**CH**OR) (*J = 6, 7, 8 and 14 Hz*), 4.46 dd (**CH$_2$**OR) (*J = 7 and 8 Hz*), 4.22 dd (**CH$_2$**OR) (*J = 7 and 8 Hz*), 3.13 dddd (**CH$_2$**) (*J = ,1, 1, 6 and 14 Hz*) 2.74 d (**CH$_2$**) (*J = 4 Hz*).
^{13}C NMR (101 MHz, DMSO-d_6). δ = 155.11 (**C**O$_3$), 135.11 (=**CH**), 118.47 (=**CH$_2$**), 75.56 (**C**HOR), 68.07 (**CH$_2$**OR), 58.24 (**CH$_2$**), 54.76 (**CH$_2$**) ppm.

The modification was carried out in two batches. First, a 8 wt% (weight-%) CNC suspension (3500 g, 280 g dry CNC) was prepared by dispersing with an Ultraturrax, in accordance with the instructions from Celluforce. To the CNC suspension, [4-((diallylamino)methyl)-1,3-dioxolan-2-one] (15.93 g, 81 mmol) was added dropwise to achieve equal molar ratios of the reagent and the sulphate half ester groups (following the surface charge information given by the supplier: 300 μmol/g). The mixture was diluted with 600 mL deionized water because it was otherwise too viscous to stir properly. The mixture was first stirred at room temperature for 8 h and then at 90 °C for 14 h with continuous stirring. The modified CNC suspension was dialyzed (Spectra/Por 2 Dialysis Membrane, MWCO 12–14 kDa) against deionized water until the conductivity in the effluent remained below 5 μS.

The composites were produced with two different polymer matrices; a low-density polyethylene (LDPE), Ineos 19N730, from Ineos Olefins and Polymers, and a poly (ethylene-acrylic acid) copolymer containing 7% acrylic acid (EAA7), Primacor 3540 from Dow Chemical Company, Sweden. The LDPE had a density of 0.92 g/cm^3, a melting point of 108 °C and a melt flow rate of 8 g/10 min (ISO 1133) according to the supplier. The EAA7 had a number average molecular weight (*M$_n$*) of 16,100 g/mol, a density of 0.932 g/cm^3, a melting point of 95 °C and a melt flow rate of 8 g/10 min (ISO 1133) according to the supplier.

2.2. Production of composites

2.2.1. Mixing and compounding
The preparation of the CNC-containing compounds was carried out as a two-step process; first a water-assisted mixing of the polymer and the CNC followed by homogenisation (compounding) extrusion. A water-assisted extrusion-based approach was used to prepare the 10 wt % CNC-containing composites. The polymer pellets and the dispersion containing CNC were simultaneously added to the hopper of the co-rotating, Werner & Pfleiderer ZSK 30 M9/2 (Stuttgart, Germany) twin-screw extruder (TSE). The dispersion containing 8 wt% unmodified CNC was added using a peristaltic pump Heidolph SP standard, PD 5001 (Schwabach, Germany) at a feed rate of 21 g/min (1.7 g dry CNC/min). The dispersion of the modified CNC, which had a solids content of 6.2 wt % and a higher viscosity, was fed through a syringe to obtain a feed rate of 27 g/min (1.6 g dry CNC/min). The feed rates of polymer pellets were adjusted to give 10 wt% CNC-containing composites. The water-assisted extrusion was carried out using the mixing screw configuration design (MS) at 50 rpm whereas the second pass, also called the compounding step, was performed using the compounding screw (CS) configuration at 70 rpm. The two different screw configurations (MS and CS) are shown in Fig. 1. The material was compounded twice in the TSE and pelletized after each cycle before being injection moulded.

The mixing screw configuration was chosen in order to convey the CNC suspension effectively, without causing excessive pooling or backflow of material towards the hopper. The compounding screw, on the other hand, had additional kneading elements to improve the dispersive and distributive mixing and break up any CNC-aggregates during the melt processing operation. The residence time was between 7 and 8 min with the MS screw configuration and 2–3 min with the CS screw configuration. The longer residence time with the MS screw configuration was due to the presence of large amounts of water which moved more slowly than the melt, and also to backflow in the extruder. The TSE used was a co-rotating twin-screw extruder, Werner &
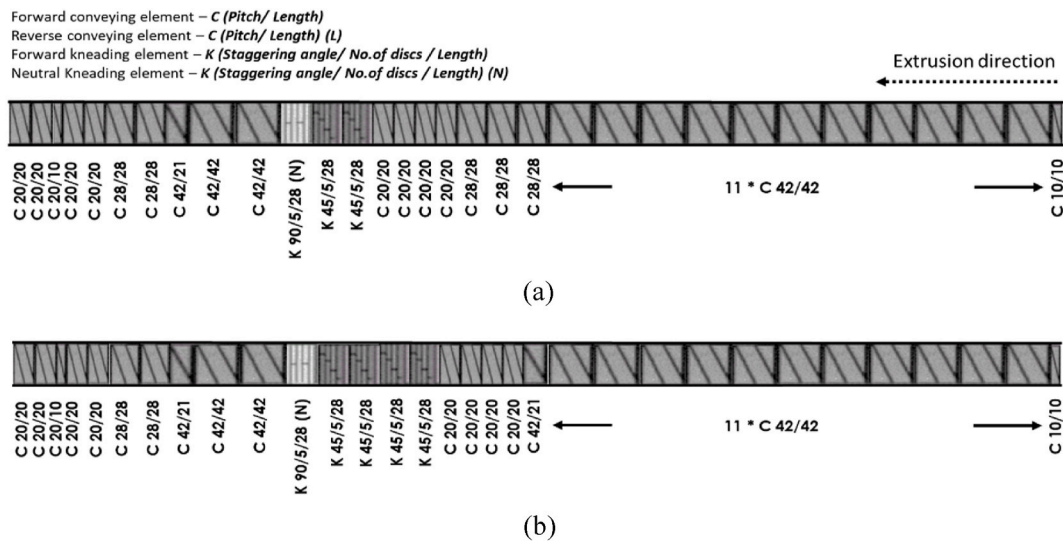
Fig. 1. The two different screw configurations; (a) Mixing screw (MS) and (b) compounding screw (CS).

Pfleiderer ZSK 30 M9/2 (Stuttgart, Germany), having a screw diameter of 30 mm and a screw length of 971 mm. The TSE had five heating zones along the cylinder and one heating zone at the end for the die. The temperature profile from the hopper to the die was 80-90-130-130-120-120 °C for the first pass (mixing step) and 120-140-200-200-170-170 °C for the second pass (compounding step). The target cellulose nanocrystal content in the composite was 10 wt%. The increase in weight due to the surface modification was less than 1% of the CNC weight and was thus considered to be negligible [29].

The 10 wt% composites were denoted on the basis of the matrix used followed by the reinforcement type, with or without diAllyl modification. For example, the sample representing EAA7 containing 10 wt% unmodified CNC was denoted 'EAA7-CNC'.

2.2.2. Injection moulding

The final shaping of the CNC-containing compounds was performed using an injection moulding machine, Arburg Allrounder 221M-250-55 (Austria), producing quadratic test plates, 64 × 64 × 1.5 mm in size. The temperature profile from the hopper to the nozzle was divided into five heating zones along the barrel; 110-150-150-170-170 °C, the injection pressure was 75 MPa, and the mould temperature was set to 25 °C. The holding pressure was 80 MPa and the backpressure was 1.5 MPa. The circumferential screw speed was set to 20 m/min. The sprue from the cylinder nozzle to the cavity diverged from a diameter of 4 mm to a diameter of 7 mm along the sprue length of 54 mm, followed by an 18 mm long runner with a cross section of 40 mm^2 and a rectangular cavity gate having a 8×1.5 mm^2 cross section and a land length of 1 mm. The injection speed was set to 50 cm^3/s while the sprue was filled and reduced to 20 cm^3/s while the mould cavity was filled. The injection moulding cycle time was 45 s, including 10 s holding time and 30 s cooling time. The first 20 samples were discarded at the start of the injection moulding series, before the process was considered stable.

2.3. Characterization methods

2.3.1. Conductometric titration

The surface charge was determined following the procedure described by Foster et al. [30]. The surface-modified sample was subjected to dialysis prior to titration, but no further pre-treatment was performed. A 100 mL 0.1 wt.-% CNC dispersion was prepared and titrated with a 10 mM sodium hydroxide solution (standardised against potassium hydrogen phthalate) by the addition of 100 μL aliquots at 30 s intervals until a sufficient number of measuring points had been

collected. The measured conductivity was corrected for the increase in volume during the measurement. The sulphate half-ester content was evaluated from the amount of sodium hydroxide required to neutralise the suspension, which was determined by the point of intersection of the slopes.

2.3.2. Attenuated total reflectance fourier transform infrared spectroscopy (ATR-FTIR)

ATR-FTIR was performed using a PerkinElmer Frontier FT-IR Spectrometer (Waltham, MA, USA) equipped with a diamond GladiATR attenuated total reflectance (ATR) attachment from Pike Technologies. The samples were placed directly on the ATR-crystal without further preparation, and the spectra were recorded between 4000 and 400 cm^{-1}, 32 scans being collected with a resolution of 2 cm^{-1} at intervals of 0.5 cm^{-1}.

2.3.3. Thermal gravimetric analysis (TGA)

Thermal gravimetric analysis was used to assess the thermal stability of the materials using a TGA/DSC 3 + Star system (Mettler Toledo, Switzerland), a 3–5 mg sample being heated at 10 °C/min from 25 to 500 °C under a nitrogen flow of 20 mL/min. The mass loss and onset temperature for degradation was calculated using the Mettler Toledo STARe evaluation software.

2.3.4. Differential scanning calorimetry (DSC)

The thermal transitions and crystallinity of the materials were assessed using a Mettler Toledo DSC2 calorimeter equipped with a HSS7 sensor and a TC-125MT intercooler. The endotherms were recorded while the temperature was increased from 25 to 160 °C at a scan rate of 10 °C/min with a nitrogen flow of 50 mL/min. No second temperature scan was used. The degree of crystallinity (X_c) was evaluated as

$$X_c = \frac{\Delta H_c}{w_{EAA}\Delta H_o} \tag{1}$$

where ΔH_c is the specific heat of fusion of the composite, w_{EAA} the weight fraction of EAA or LDPE and ΔH_o the specific heat of fusion of 100% crystalline polyethylene; 277.1 J/g [31]. The melting point (T_m) of the polymer matrix was taken as the peak value of the DSC endotherm.

2.3.5. Appearance

The colour of the injection-moulded plaques was assessed using a Datacolor 600 d/8° spectrophotometer with a 9 mm diameter opening.

The colour was expressed in the 1976 CIELAB system [32] with co-ordinates L* (lightness), a* (red-green) and b* (yellow-blue). The lightness L* ranges from 0 (black) to 100 (white), -a* is green, +a* red, -b* is blue and +b* yellow. The measurements were performed with a white paper background to provide equivalent conditions for the semi-transparent samples. Each reported value was the average of three measurements at different positions on a plaque.

The gloss was measured with a Konica Minolta Uni Gloss 60 Plus having an incidence angle of 60° at room temperature. To ensure equivalent conditions, a white paper background was used, and the gloss of this paper was also measured. The reported values are averages of three measurements, all performed with the incident light beam perpendicular to the main direction of the melt.

2.3.6. Mechanical properties

A Zwick/Z2.5 tensile tester equipped with a 2 kN load cell was used to measure the tensile properties of the materials. Bars with a gauge length of 40 mm were cut from the mid-section of the injection-moulded plaques, with the length oriented in the injection direction. One test bar was cut from each plaque and conditioned at 23 ± 2 °C and $53 \pm 2\%$ relative humidity for 48 h prior to the tensile test. The Young's modulus, tensile strength at yield, elongation at yield, ultimate tensile strength and elongation at break were measured at 25 °C with a strain rate of 2.5×10^{-3} s^{-1} (6 mm/min). The reported values are the average values of five independent measurements.

2.3.7. Dynamic-mechanical analysis

A Rheometrics RSA II was used to measure the dynamic-mechanical properties of the materials at room temperature. Specimens were cut out from the mid-section of the injection-moulded plaques in the direction of injection and conditioned at 23 ± 2 °C and $53 \pm 2\%$ relative humidity for 48 h prior to the measurement. The specimens were strained in tension to about 0.13% and this strain was kept constant while a sinusoidal deformation was superimposed at a temperature of 23 °C. The measured loss and storage moduli of the materials were recorded.

2.3.8. Rheological properties

The shear viscosity of the melts was determined as a function of the shear rate using a capillary viscometer (Göttfert Rheograph 2002, Germany). Two cylindrical capillaries of different lengths (10 and 20 mm) but with the same diameter (1 mm) were used in order to make it possible to estimate the pressure entrance losses (Bagley correction of the applied pressure). A 500 bar (50 MPa) pressure transducer (Dynisco, USA) was used to record the pressure applied when the melt was pushed through the capillary at different speeds. The piston speed was varied between 0.05 and 2 mm/s, corresponding to shear rates of 58–2300 s^{-1}. The measured shear rates were subjected to a Rabinowitch-correction. The shear viscosities were determined at a melt temperature of 170 °C.

Small-amplitude oscillatory shear tests (SAOS) were performed on the extruded samples at 170 °C using an Anton Paar MCR 702 rheometer (Graz, Austria) with parallel plate geometry (15 mm plate diameter). The disk-shaped samples, with a thickness of 1.5 mm, were gradually squeezed to a plate gap of 1 mm. The rheological properties of the composites were found to be stable at 170 °C for a period of more than 50 min, so that thermal degradation during the rheological measurements was considered to be negligible. In the SAOS experiments, the linear viscoelastic region was first assessed using a strain sweep from 1 to 100% at a constant angular frequency of 1 s^{-1}. In addition, angular frequency sweeps were made in the range of 0.08–200 s^{-1} at strain amplitudes of 0.04–0.7%. In most cases, the experiments were repeated twice on different specimens.

3. Results and discussion

3.1. Synthesis

Both the unmodified CNC and the diallyl-modified CNC, modified using azetidinium salts, have been extensively characterised in previous papers [25,26]. A deeper description of the route for the production of N-diAllyl-carbonate used here will be published later.

The chemical modification achieved was characterised using TGA, FTIR and conductometric titration. The temperature of onset of thermal degradation was, as expected slightly higher for the modified than for to the unmodified CNC, as can be seen in Table 2, indicating stabilisation of the sulphate groups through covalent surface functionalisation. FTIR showed the typical peaks for nanocellulose; a broad band at 3600-3100 cm^{-1} attributed to O–H stretching, a band at ca. 2899 cm^{-1} attributed to aliphatic C–H stretching, a band at 1429 cm^{-1} attributed to CH$_2$ scissoring in cellulose I, bands at 1162 cm^{-1} and 898 cm^{-1} typical of the glycosidic bond, bands at ca. 1030 cm^{-1} attributed to C–O stretching, as well as the characteristic band at 809 cm^{-1} attributed to the C–O–S stretching associated with sulphate ester groups. Conductometric titration showed the presence of weak basic groups at a concentration of 151 mmol/kg, compared with 250–300 mmol/kg for the unmodified CNC from CelluForce, and no acidic surface groups [33]. FTIR and conductometric titration results are available in the supplementary information as Figs. S1 and S2 respectively. The lack of acidic surface groups shown by conductometric titration together with the presence of C–O–S bonds indicated by FTIR confirm the modification of the sulphate, supported by the presence of weak basic groups and a high thermal stability. The results of the conductometric titration indicate that all the sulphate half esters on the CNC surface were functionalised.

3.2. Water-assisted mixing, compounding and injection moulding

The wet mixing of the CNC dispersion and the polymer pellets in the TSE followed by the secondary compounding step and the injection moulding were successfully performed. The processing parameters and possible difficulties when upscaling the production to a continuous operation were taken into consideration through several trials. Various combinations of process temperature, screw design, screw speed, feeding position and feeding rate of the CNC were tested to obtain a steady process. The injection-moulding process was adjusted in terms of temperature, injection speed and holding pressure to achieve homogeneous plaques without excessive internal stresses, shrinkage or flash.

3.3. Appearance

Visual inspection of the injection-moulded plaques revealed a change in transparency and colour due to the addition of the CNC, as shown in Fig. 2. Small darker entities, indicating agglomeration of CNC in the material were also observed. This was more pronounced in the EAA7 samples and the colour difference was greater with the EAA7 as matrix. This was possibly due to the presence of carboxylic acid groups in EAA7, causing an initiation of degradation, previously discussed by Forsgren et al. where a EAA15 composite with CNC did not show this darkening effect when being pH neutralized [11].

The colour and gloss values for the different samples are summarized in Table 1. A clear reduction in lightness (L*) is seen for both EAA7 and LDPE composites compared to the unfilled matrix. This decrease was greater in the EAA7 composite, as is evident in Fig. 2. All the reinforced samples were significantly more yellow than the neat matrices, as indicated by the *b** coordinate. The a* coordinate shows that the addition of CNC to EAA7 resulted in a somewhat increased redness. The changes in the case of the LDPE material were smaller and indicate a slight increase in greenness. All the specimens exhibited similar gloss values, but a slight decrease in gloss was noted for the composites. This may be due to a slightly rougher surface [34]. The small variations in
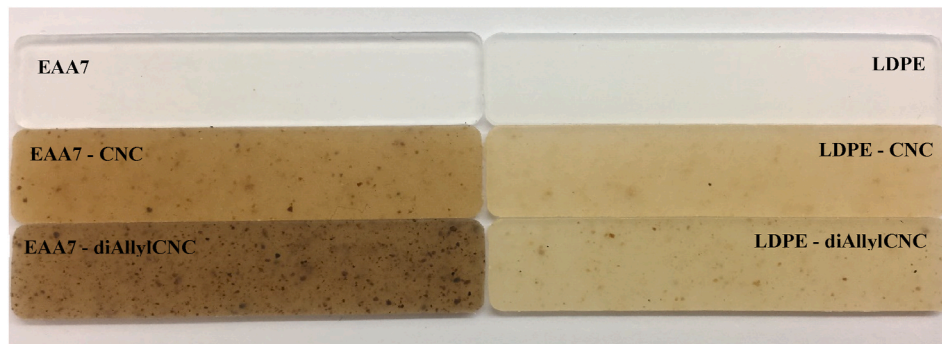
Fig. 2. The injection-moulded samples of EAA7 and LDPE reinforced with 10% unmodified or diallyl-modified CNC.

Table 1
The colour coordinates and gloss values, with standard deviation, of the unfilled polymer matrices and the composite materials, measured on injection-moulded plaques.

Sample	CIEL*	CIEa*	CIEb*	Gloss (%)
EAA7	84.0 (0.1)	2.5 (0)	−3.5 (0.1)	26.9 (3.7)
EAA7-CNC	58.9 (0.1)	4.7 (0)	21.3 (0.1)	19.9 (0.8)
EAA7-diAllylCNC	52.2 (0.9)	6.0 (0.2)	19.2 (0.3)	21.7 (1.8)
LDPE	77.3 (0.5)	2.6 (0.1)	−4.6 (0.3)	26.7 (1.0)
LDPE-CNC	68.2 (0.7)	2.2 (0.2)	13.2 (0.7)	22.8 (2.2)
LDPE-diAllylCNC	69.1 (0.3)	0.9 (0.1)	13.2 (0.6)	26.1 (2.4)

gloss may indicate that the surface topography was mainly governed by replication of the mould surface.

3.4. Thermal properties

Neither the crystallinity nor the melting point was significantly changed by the addition of CNC, regardless of the type of CNC added, as can be seen in Table 2.

Table 2 and Fig. 3 include the onset temperatures for the degradation (T_{onset}) of the unmodified and modified CNC dried into thin films from the original dispersion, the neat polymer matrices and the composites. Table 2 presents two temperatures for the composites, the lower associated with the degradation of CNC and the higher with that of the polymer matrix. Although the dried unmodified CNC films were slightly less thermally stable than their modified counterparts, the opposite was noted for the composites. The composites reinforced with unmodified CNC exhibited a higher thermal stability (approx. 240 °C) than the composites reinforced with the modified CNC (240 °C). The degradation temperature of the unmodified CNC was here higher than that reported by Forsgren et al. possibly due to the different CNC grade used [11]. The Celluforce CNC used in this work is significantly more stable because it is Na$^+$ ion-neutralized since it occurs in the form of a re-dispersible spray-dried powder [35].

Table 2
The degree of crystallinity, melt temperature and onset temperature for thermal degradation with standard deviations for the neat CNC's dried into films, the neat polymer matrices and the composites.

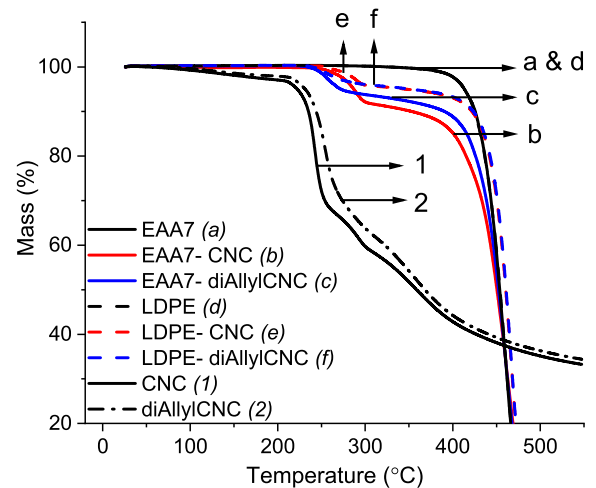| Material	Crystallinity (%)	Melting point (°C)	T_{onset} (°C)
CNC	–	–	236 (2)
diAllylCNC	–	–	238 (2)
EAA7	16 (1.0)	98 (2)	430 (3)
EAA7-CNC	16 (1.1)	99 (1)	265 (5); 415 (5)
EAA7-diAllylCNC	14 (0.1)	99 (1)	239 (3); 419 (5)
LDPE	22 (0.6)	108 (2)	441 (4)
LDPE-CNC	21 (0.6)	109 (2)	272 (4); 436 (4)
LDPE-diAllylCNC	20 (0.9)	108 (3)	238 (3); 437 (2)

Fig. 3. Thermogravimetric curves showing the thermal degradation of the neat CNC's, unmodified and modified, the neat polymer matrices and the composites.

3.5. Mechanical properties

The results of the tensile tests are summarized in Table 3. In both matrices, the addition of CNC markedly increased the Young's modulus and yield stress of the materials, as expected and desired. Although the magnitude of the increase was somewhat smaller than earlier reported results for similar composites [11]. This may be due to the different CNC grade used or to the difference in the manufacturing techniques. Forsgren et al. used compression moulding, and the flow behaviour in injection moulding probably affected the morphology and behaviour of the samples [36]. The surface treatment of CNC did not, however, result in any increase in the modulus or in the yield strength compared to the unmodified CNC, which was somewhat surprising. The addition of diallyl-modified CNC increased the modulus of the EAA7-composites by about 50%, but the unmodified CNC increased the modulus to almost 100%, possibly because the reduced interaction of hydrogen bonds between EAA7 and modified CNC due to the surface grafting had a plasticizing effect. The EAA7-unmodified CNC composite also showed the greatest increase in yield stress when the CNC was added, with an increase of more than 100%. With the LDPE as matrix, the modified–CNC– and unmodified–CNC–based samples behaved similarly, with little difference between the stiffnesses and strengths of the composites.

In all cases, the addition of CNC had little effect on the ultimate tensile strength, but the addition of the nanocrystals greatly lowered the elongation at break, but the EAA7 containing diallyl-modified CNC was the most ductile of the composites, which again possibly indicates a plasticizing effect. The addition of the unmodified CNC to EAA7 resulted in the greatest increase in stiffness and yield stress, but the EAA7-

Table 3
Tensile properties of the injection-moulded composites. Each value reported is an average of 5–6 measurements, with the standard deviation in brackets.

Sample	Young's modulus (MPa)	Yield stress (MPa)	Ultimate tensile strength (MPa)	Elongation at break (%)
EAA7	109 (2)	5.7 (0.1)	16.8 (0.6)	90.6 (2.6)
EAA7-CNC	207 (4)	12.9 (0.3)	17.5 (0.3)	36.7 (3.6)
EAA7-diAllylCNC	166 (4)	8 (0.2)	16 (0.5)	59 (3.2)
LDPE	150 (7)	7 (0.1)	13 (0.3)	62 (3.6)
LDPE-CNC	210 (2)	8.5 (0.3)	12.1 (0.3)	39.4 (1)
LDPE-diAllylCNC	209 (6)	9 (0.2)	12.6 (0.1)	38 (2.1)

diAllylCNC composite showed a greater elongation at break, providing a somewhat stronger material than the matrix but retaining some of its ductility.

3.6. Dynamic-mechanical analysis (DMA)

Fig. 4 shows the mechanical loss factor (tan δ) as a function of the amplitude of the sinusoidal deformation. The difference in slope of the loss factor curve between the composite and the matrix provides information about the interphase between the matrix and the reinforcement [11,37,38]. The EAA7-based samples containing unmodified and modified CNC exhibited a plateau in loss factor at low strain amplitudes, but with increasing strain amplitude, the loss factor value increased. This increase was more pronounced when the EAA7 was reinforced with the unmodified than with the modified CNC, which suggests that the surface treatment in this case created a more stable interphase region. This hypothesis is to some extent supported by the greater extensibility of the composite, cf Table 3. Forsgren et al. also showed that the diAllyl-treatment gave a more stable interphase region [11]. With LDPE as the matrix, the loss factor of the composites increased somewhat more than that of the unfilled polymer and there was no significant difference between the modified or unmodified CNC.

3.7. Rheological properties

Fig. 5 shows the shear viscosity of the melts at 170 °C as a function of the shear rate, after application of the Bagley and Rabinowitch corrections. The shear viscosities of the different melts exhibited rather similar behaviours, but they differed in magnitude. In all cases, a shear-thinning behaviour was observed. The EAA7-based melts exhibited a somewhat higher viscosity than those based on LDPE. The addition of CNC to EAA7 resulted in an increase in viscosity at a given shear rate compared to the unfilled polymer, and the surface treatment of the CNC appeared to reduce the viscosity slightly relative to that of the melt containing
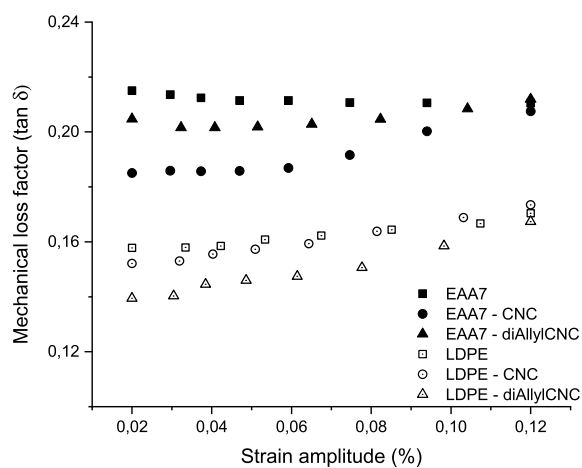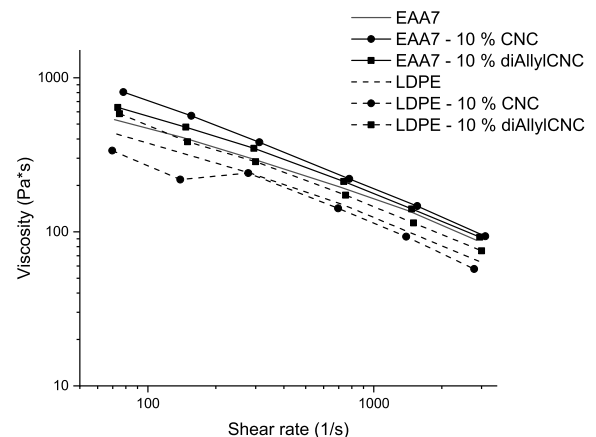

Fig. 5. The shear viscosity of the melts as a function of shear rate after applying Bagley and Rabinowitch corrections.

untreated CNC. This may be related to a plasticizing effect of the surface treatment and a less developed filler network as discussed previously. The viscosities of the LDPE-based melts were similar but the melt containing the surface-treated nanocellulose had the highest viscosity.

The results of the oscillatory shear experiments, strain sweep and frequency sweep, are summarized in Fig. 6. For the oscillatory strain sweep, Fig. 6a, the samples exhibited a storage modulus (G') plateau over the entire range of applied shear strain, except for the EAA7-CNC-, and EAA7-diAllylCNC-based samples. The EAA7-based samples containing the unmodified CNC had a higher G' than those containing the surface-treated CNC. This follows the pattern noted for Young's modulus (Table 3) and is possibly explained by a more developed percolated cellulose network in the EAA7-unmodified CNC composite. Fibril−fibril interactions such as hydrogen bonding are expected to act as cohesive forces and contribute to the network strength, and thus affect the stiffness and elongation at break [39]. Surface grafting may interfere with these interactions and thus affect the strength of the network. Both the unmodified and modified CNC-reinforced samples exhibited an increasing G' with increasing strain amplitude up to a certain critical shear strain value, after which it decreased. This overshoot of G' has previously been observed in polymers or complex systems with a structural network which resists deformation up to a certain critical strain [40,41]. In the present case, the overshoot was observed only for the G' while the loss modulus G'' remained constant. The LDPE-based composites exhibited no such behaviour and the CNC-reinforced samples exhibited lower G' values than the matrix polymer, the samples containing the unmodified CNC having the lowest values.

In the frequency sweep, as shown in Fig. 6b, the EAA7-based samples containing CNC clearly differed. The samples exhibited a plateau at lower frequencies and the EAA7 containing unmodified CNC showed the highest G' values. A plateau at lower frequencies is observed in systems having a structural network [15,42,43]. No such plateau was observed for the LDPE samples reinforced with CNC; they behaved in a manner similar to that of the matrix material, and they displayed lower G' values than the unfilled LDPE. This behaviour was also visible in the

Fig. 4. The mechanical loss factor (tan δ) as a function of applied strain amplitude for LDPE (unfilled symbols) and EAA (solid symbols) reinforced with 10 wt% unmodified-(circles) and modified-(triangles) CNC.
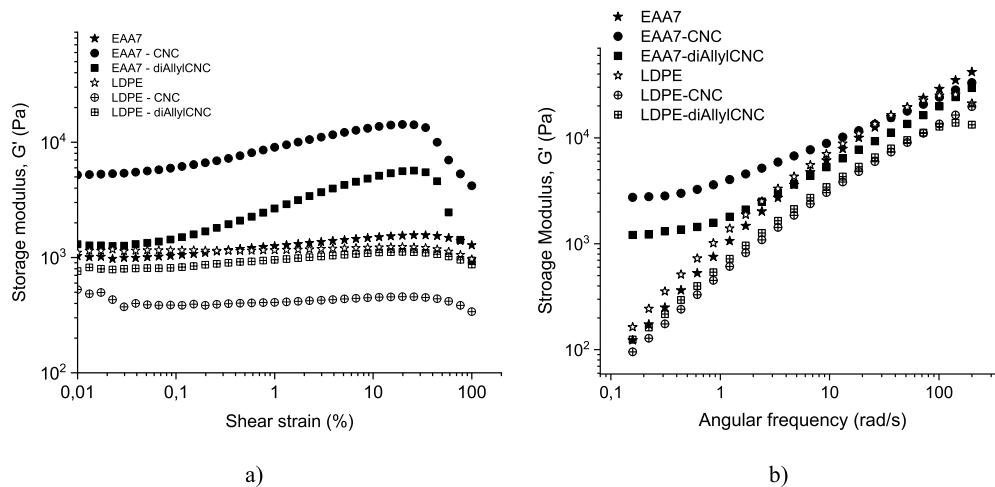
Fig. 6. The storage moduli (G′) as a function of (a) shear strain amplitude and (b) angular frequency for EAA (filled symbols) and LDPE (unfilled symbols) composites reinforced with unmodified and modified CNC.

mechanical properties of the material. There was little variation in the strength of the LDPE composites reinforced with CNC, which could be related to the absence of a percolated network in the material.

4. Conclusions

This study has successfully achieved the continuous and relatively large-scale manufacture of CNC (neat and surface-treated)-containing composites based on aqueous mixing in a twin-screw extruder followed by injection moulding. Both EAA- and LDPE-based composites were produced in this manner. Further optimization of the process may be required to reduce local temperature increases in the manufacturing equipment and to shorten the residence time in order to further reduce the discoloration and thermal degradation of the material.

The addition of 10% CNC to the matrix materials increased the stiffness and yield strength of the polymers, the effect being more pronounced in the case of EAA7 matrix, partly because the values of the EAA7 polymer were lower than those of the LDPE. In view of earlier findings (Forsgren et al., 2019), the surface treatment was somewhat less effective than expected, especially with regard to its effect on the yield strength. There may be several reasons for this; the unmodified CNC was of a different grade, the surface treatment procedure was modified and the processing was harsher. There are also indications that the surface treatment of the CNC induced a plasticization of the EAA polymer, which may be an advantage in some situations. Further studies should shed some more light on this.

It was expected that a more hydrophilic polymer such as EAA would promote the dispersion of the CNC in the matrix but this was not the case, not even for the surface-treated CNC, as supported by the photographs shown in Fig. 2., the viscosity measurements in Fig. 5 and the mechanical properties in Table 3. In contrast to the results of the previous work by Forsgren et al. the modification of the CNC did not significantly increase the thermal stability, but this may be due to the use of more thermally stable unmodified CNC grade in this work. The significant browning of the EAA7 composites containing modified CNC was possibly due to the presence of carboxylic acid groups in the EAA7 melt causing degradation and the discoloration of the specimens. The thermal resistance depends strongly on the residence time and the temperature of the melt exiting the nozzle can be significantly different from the actual settings due e.g. to viscous heating causing discoloration of the material even at a set processing temperature of 170 °C. Colour changes are however a sensitive measurement giving an early indication of degradation that is not necessarily connected to a decrease in mechanical strength [4,34].

The strain and frequency sweep experiments on the melts strongly suggested that a percolated filler network structure was formed when CNC, whether unmodified or modified, was added to EAA7, but this did not take place with LDPE as matrix. This suggests interactions between the EAA polymer and the CNC, which was supported by the slightly higher shear viscosity of the reinforced EAA7 than that of the LDPE samples and the pure EAA7 matrix. Composites with LDPE as matrix material did not show any network formation.

The DMA results show a stronger interphase region between the CNC and EAA7 than when LDPE was used as the matrix material. The EAA7-diAllylCNC in particularly indicated a stronger interphase region, which is supported by the large elongation at break for this material.

Credit author statement

Lilian Forsgren: Conceptualization, Writing – original draft, Investigation, Visualization, Methodology, Validation, Writing – review & editing Abhijit Venkatesh: Conceptualization, Writing – original draft, Investigation, Visualization, Methodology, Validation, Writing – review & editing Florian Rigoulet: Investigation, Methodology, Validation Karin Sahlin-Sjövold: Conceptualization, Methodology, Validation, Writing – review & editing Gunnar Westman: Supervision, Conceptualization, Methodology, Writing – review & editing Mikael Rigdahl: Supervision, Conceptualization, Methodology, Writing – review & editing Antal Boldizar: Supervision, Conceptualization, Methodology, Writing – review & editing.

Declaration of competing interest

The authors declare that they have no known competing financial interests or personal relationships that could have appeared to influence the work reported in this paper.

Acknowledgements

Appendix A. Supplementary data

Supplementary data to this article can be found online at https://doi.org/10.1016/j.compositesb.2020.108590.

References

[1] Saito T, Kimura S, Nishiyama Y, Isogai A. Cellulose nanofibers prepared by TEMPO-mediated oxidation of native cellulose. Biomacromolecules 2007;8: 2485–91.

[2] Berglund LA, Peijs T. Cellulose biocomposites—from bulk moldings to nanostructured systems. MRS Bull 2010;35:201–7.

[3] Berggren K/, Klason C, Kubat, Spritzgiessen J. Holzmehlhaltiger Thermoplaste. Kunststoffe 1975;65:69–74.

[4] Dalväg H, Klason C, Strömvall H-E. The efficiency of cellulosic fillers in common thermoplastics. Part II. Filling with processing aids and coupling agents. Int. J. Polym. Mater. Polym. Biomater. 1985;11:9–38.

[5] Kokta BV, Chen R, Daneault C, Valade JL. Use of wood fibers in thermoplastic composites. Polym Compos 1983;4:229–32.

[6] Hans Domininghaus. Plastics for engineers: materials, properties, applications - hans domininghaus - google books. Hans Gardner Publications; 1993.

[7] Miao C, Hamad WY. Cellulose reinforced polymer composites and nanocomposites: a critical review. Cellulose 2013;20:2221–62.

[8] Pickering KL, Efendy MGA, Le TM. A review of recent developments in natural fibre composites and their mechanical performance. Composites Part A Appl Sci Manuf 2016;83:98–112.

[9] Lee KY, Aitomäki Y, Berglund LA, Oksman K, Bismarck A. On the use of nanocellulose as reinforcement in polymer matrix composites. Compos Sci Technol 2014;105:15–27.

[10] Azizi Samir MAS, Alloin F, Sanchez J-Y, Dufresne A. Cellulose nanocrystals reinforced poly(oxyethylene). Polymer 2004;45:4149–57.

[11] Forsgren L, et al. Composites with surface-grafted cellulose nanocrystals (CNC). J Mater Sci 2019;54:3009–22.

[12] Oksman K, et al. Review of the recent developments in cellulose nanocomposite processing. Composites Part A Appl Sci Manuf 2016;83:2–18.

[13] Zheng T, Pilla S. Melt processing of cellulose nanocrystal-filled composites: toward reinforcement and foam nucleation. Ind Eng Chem Res 2020;59:8511–31.

[14] Boldizar A, Klason C, Kubát J, Näslund P, Sáha P. Prehydrolyzed cellulose as reinforcing filler for thermoplastics. Int J Polym Mater 1987;11:229–62.

[15] Venkatesh A, Thunberg J, Sahlin-Sjövold K, Rigdahl M, Boldizar A. Melt processing of ethylene-acrylic acid copolymer composites reinforced with nanocellulose. Polym Eng Sci 2020;60:956–67.

[16] Azouz K Ben, Ramires EC, Van Den Fonteyne W, El Kissi N, Dufresne A. Simple method for the melt extrusion of a cellulose nanocrystal reinforced hydrophobic polymer. ACS Macro Lett 2012;1:236–40.

[17] Herrera N, Mathew AP, Oksman K. Plasticized polylactic acid/cellulose nanocomposites prepared using melt-extrusion and liquid feeding: mechanical, thermal and optical properties. Compos Sci Technol 2015;106:149–55.

[18] Herrera N, Salaberria AM, Mathew AP, Oksman K. Plasticized polylactic acid nanocomposite films with cellulose and chitin nanocrystals prepared using extrusion and compression molding with two cooling rates: effects on mechanical, thermal and optical properties. Composites Part A Appl Sci Manuf 2016. https://doi.org/10.1016/j.compositesa.2015.05.024.

[19] Peng J, Walsh PJ, Sabo RC, Turng L-S, Clemons CM. Water-assisted compounding of cellulose nanocrystals into polyamide 6 for use as a nucleating agent for microcellular foaming. Polymer 2016;84:158–66.

[20] Karger-Kocsis J, Kmetty Á, Lendvai L, Drakopoulos S, Bárány T. Water-assisted production of thermoplastic nanocomposites: a review. Materials 2014;8:72–95.

[21] Yasim-Anuar TAT, et al. Well-dispersed cellulose nanofiber in low density polyethylene nanocomposite by liquid-assisted extrusion. Polymers 2020;12:927.

[22] Trejo-O'Reilly J-A, Cavaille J-Y, Gandini A. The surface chemical modification of cellulosic fibres in view of their use in composite materials. Cellulose 1997;4: 305–20.

[23] George J, Sreekala MS, Thomas S. A review on interface modification and characterization of natural fiber reinforced plastic composites. Polym Eng Sci 2001;41:1471–85.

[24] Baiardo M, Frisoni G, Scandola M, Licciardello A. Surface chemical modification of natural cellulose fibers. J Appl Polym Sci 2002;83:38–45.

[25] Börjesson M, Sahlin K, Bernin D, Westman G. Increased thermal stability of nanocellulose composites by functionalization of the sulfate groups on cellulose nanocrystals by azetidinium ions. J Appl Polym Sci 2018;135:45963.

[26] Sahlin K, et al. Surface treatment of cellulose nanocrystals (CNC): effects on dispersion rheology. Cellulose 2018;25:331–45.

[27] Krishna Reddy VVRM, et al. Development of an optimized process for the preparation of 1-Benzylazetidin-3-ol: an industrially important intermediate for substituted azetidine. Org Process Res Dev 2011;15:462–6.

[28] Parzuchowski PG, Świderska A, Roguszewska M, Frączkowski T, Tryznowski M. Amine functionalized polyglycerols obtained by copolymerization of cyclic carbonate monomers. Polymer 2018;151:250–60.

[29] Dong XM, Revol JF, Gray DG. Effect of microcrystallite preparation conditions on the formation of colloid crystals of cellulose. Cellulose 1998;5:19–32.

[30] Foster EJ, et al. Current characterization methods for cellulose nanomaterials. Chem Soc Rev 2018;47:2609–79.

[31] J Brandup EI. In: E. G. Polymer handbook. fourth ed., vol. 49. Wiley-Blackwell; 1999. Polymer international.

[32] Iso/Cie 11664-4:2019. International commission on illumination 8. https://www.techstreet.com/cie/standards/iso-cie-11664-4-2019?gateway_code=cie&product_id=2078733#jumps; 2019.

[33] Reid MS, Villalobos M, Cranston ED. Benchmarking cellulose nanocrystals: from the laboratory to industrial production. Langmuir 2017;33:1583–98.

[34] Forsgren L, Berglund J, Thunberg J, Rigdahl M, Boldizar A. Injection molding and appearance of cellulose-reinforced composites. Polym Eng Sci 2020;60:5–12.

[35] Roman Maren, William T, Winter *. Effect of sulfate groups from sulfuric acid hydrolysis on the thermal degradation behavior of bacterial cellulose. Biomacromolecules 2004;5:1671–7.

[36] Nagalakshmaiah M, Pignon F, El Kissi N, Dufresne A. Surface adsorption of triblock copolymer (PEO-PPO-PEO) on cellulose nanocrystals and their melt extrusion with polyethylene. RSC Adv 2016;6:66224–32.

[37] Kubát J, Rigdahl M, Welander M. Characterization of interfacial interactions in high density polyethylene filled with glass spheres using dynamic-mechanical analysis. J Appl Polym Sci 1990;39:1527–39.

[38] Nielsen LE. Mechanical properties of polymers and composites -, vol. 2. M. Dekker; 1994.

[39] Peterson A, et al. Dynamic nanocellulose networks for thermoset-like yet recyclable plastics with a high melt stiffness and creep resistance. Biomacromolecules 2019;20:3924–32.

[40] Chen Y, Xu C, Huang J, Wu D, Lv Q. Rheological properties of nanocrystalline cellulose suspensions. Carbohydr Polym 2017;157:303–10.

[41] Townsend AK, Wilson HJ. Small- and large-amplitude oscillatory rheometry with bead–spring dumbbells in Stokesian Dynamics to mimic viscoelasticity. J. Nonnewton. Fluid Mech. 2018;261:136–52.

[42] Khoshkava V, Kamal MR. Effect of cellulose nanocrystals (CNC) particle morphology on dispersion and rheological and mechanical properties of polypropylene/CNC nanocomposites. ACS Appl Mater Interfaces 2014;6:8146–57.

[43] Sharif-Pakdaman A, Morshedian J, Jahani Y. Influence of the silane grafting of polyethylene on the morphology, barrier, thermal, and rheological properties of high-density polyethylene/organoclay nanocomposites. J Appl Polym Sci 2012; 125:E305–13.